A new mathematical tool for analyzing the fracturing process in rock: Partial symmetropy of microfracturing

Yamasaki, K.

Nanjo, K. Z.

(Citation)
Physics of the Earth and Planetary Interiors,173(3-4):297-305

(Issue Date)
2009-04

(Resource Type)
journal article

(Version)
Accepted Manuscript

A new mathematical tool for analyzing the fracturing process in rock: Partial symmetropy of microfracturing

K. Yamasaki[a,*], K. Z. Nanjo[b]

[a] *Department of Earth and Planetary Sciences, Faculty of Science, Kobe University, Nada, Kobe 657-8501, Japan*

[b] *Swiss Seismological Service, ETH Hoenggerberg, HPP P, 8093 Zurich, Switzerland*

Abstract

We have shown that the symmetry of fracturing process in a macro scale can be quantified by using the concept of symmetropy (an entropy-like measure of symmetry). Here we extend this approach to examining the symmetries in a range from small (partial) scales to larger (whole) scales: This approach is called partial symmetropy (PS). To check its applicability, we consider one illustrative example, the temporal change of the spatial patterns of acoustic-emission events in a well-documented rock fracture experiment. Our results are summarized as follows: (i) The PS enables us to distinguish the nucleation phases from the other phases such as the pre-nucleation and the propagation phases; (ii) The variation of the PS shows that the fracturing process is a associated with a type of phase transitions from the subcritical state to the critical state; (iii) The scale dependence of the PS reveals the presence of the sandwich structure that consists of order and non-order in the evolution of the fracturing pattern; (iv) Within the framework of nonextensive Tsallis entropy we develop the PS concept, and show that the degree of nonextensivity on a large scale increases immediately after the nucleation. The results shown in the present paper are not obtained by taking the traditional fractal

*Corresponding author. *E-mail address:* yk2000@kobe-u.ac.jp (K. Yamasaki).

approach, nor using only a simply symmetropy. We therefore propose that the PS is a useful tool to providing a strategy for describing qualitatively the phase changes in the observed fracturing process.

keywords: symmetropy; symmetry; Tsallis entropy; fracturing process; fractal; Walsh analysis

1 Introduction

There are many kinds of phenomena in nature which display scale symmetry characterized by fractal (Mandelbrot, 1982; Turcotte, 1997). For instance, phase transitions such as fracturing process, consists of pre-nucleation, nucleation and propagation phase (e.g., Lockner et al., 1992), have a statistical scale symmetry structure over a wide range of size scales through the fractal (e.g., Ito and Matsuzaki, 1990). This fractal fracturing, i.e., the evolution of scale symmetry has been recognized as entropy relaxation process (e.g., Enya, 1901; Ito and Matsuzaki, 1990). It is one of the remaining issues to adapt the general connection between symmetry and entropic form to measure information about systems having particular symmetry (Tsallis, 2002). Nanjo et al., (2000) have examined the fracturing process based on entropy-like measure of symmetry, i.e., symmetropy (Yodogawa, 1982). This symmetropy approach is a useful tool for the quantification of anisotropy, asymmetry and entropic heterogeneity of fracturing patterns (Nanjo et. al., 2005; 2006).

One of the unique features of the fractal analysis is to enlarge or reduce the scale of observation windows. Such a critical comparison of a large scale (a whole) versus a small scale (parts) will better enable us to find out an essential feature of a geometrical pattern. In the previous study (e.g., Nanjo et al., 2000; 2005; 2006), however, only a whole symmetropy of fracturing patterns has been considered. That is, the relationship between a whole symmetropy and a partial symmetropy (PS) has not been discussed. Then, we consider the PS of fracturing patterns on a multiscale. This is a main purpose of the present paper. For this analysis, we use the data on the spatial pattern of acoustic-emission events in a rock-microfracture experiment (Lockner et al., 1992).

As we will see, this PS approach yields new insights into geophysics: (i) the nucleation phase of the fracturing process within rocks can be distinguished from the other phases by noting the PS; (ii) The fracturing process is a type of phase transitions from the subcritical state to the critical states. In this case, the subcritical and the critical states correspond to the pre-nucleation and the propagation phases, respectively; (iii) In the evolution of the fracturing pattern, the sandwich structure consists of order and non-order can be observed.

Now, it has been a problem whether a system as a whole is just a collection of subsystems as parts. If the subsystems dependent each other, it creates a possibility that the system is not just a collection of them. This is closely related to the property of entropy such as extensivity, namely proportionality with the number of subsystems of the system (Kalimeri et al., 2008). The Boltzmann-Gibbs (B-G) entropy satisfies this prescription if the subsystems are statistically (quasi-)independent, or typically if the correlations within the system are essentially local (Kalimeri et al., 2008). In such cases, the system is called extensive. In general, however, the B-G entropy may be nonextensive in the case that correlations may be far negligible at all scales. According to Kalimeri et al., (2008), the fracturing process is thought to be nonextensive situations. Then, in this paper, we extend the concept of the PS to include the effect of the nonextensivity. To do this, we use the Tsallis statistics that proposes a generalization of the B-G statistical mechanics inspired by multifractal concepts (Tsallis, 1988; 2002; Kalimeri et al., 2008; Papadimitriou et al., 2008; Contoyiannis and Eftaxias, 2008).

The structure of this paper is as follows. In Section 2, we explain data on fracturing process and methods for calculating the PS. In Section 3, we describe results. In Section 4, we discuss results and reconsider the fracturing process in terms of Tsallis statistics.

2 Data and Methods

2.1 Data

In order to estimate PS and fractal dimensions of fracture patters, we use the spatial patterns of acoustic emission (AE) events generated by microfracturings within rock. Nanjo et al., (2000) showed that the symmetropy of AE (acoustic emission) patterns decreases with the evolution of the fracturing process. For this analysis, Nanjo et al., (2000) used Hirata et al., (1987)'s data, in which a constant stress fracture experiment of Oshima granite was carried out at the confining pressure of 40 MPa. Although this result is valuable for the basic research on predicting earthquakes, it is unclear which of the AE patterns in Hirata et al., (1987)'s data corresponds to which of the fracturing phases such as pre-nucleation, nucleation and propagation. Then, in this paper, we used the data published in Lockiner et al., (1992), because these data are enough to show the consecutive process of fracture growth as shown in Fig. 1. In Lockner et al., (1992), a constant stress fracture experiment of Westerly granite was carried out at the confining pressure of 50±0.2 MPa. We use plots of AE locations for sample G1 that is view looking along-strike of eventual fracture plane.

2.2 Methods I: Fractal analysis and Walsh analysis

In order to analyze the fractal structure of fracture process, we estimate the fractal dimensions of AE patterns. For this analysis, we use a standard box-counting method (e.g., Mandelbrot, 1982; Nanjo and Nagahama, 2004). An AE pattern is overlaid with a grid of square boxes; grids of different size boxes are used. The number of boxes $N(r)$ of size r required to cover the AE pattern is plotted on the double logarithmic graph as a function of r. If the AE patten has a self-similar structure, then we derive the following relations:

$$N(r) \propto r^{-D}, \tag{1}$$

where D is defined as fractal dimension (box-counting dimension). In this study, D is given by the slope of the least-square regression line fitted to data within an effective range on the double logarithmic graph.

On the other hand, to estimate symmetry and entropy of fracture process, we use discrete Walsh analysis and the concept of symmetropy. As details of the mathematical procedures were given in a previous paper (Nanjo et al., 2006; Nishiyama et al., 2008), only a brief outline is described below.

Patterns used in this paper are restricted to a rectangular matrix, each consisting of $G \times H$ rectangular cells, where G=2^y and H=2^z (y and z are positive integers). The two-dimensional discrete Walsh transform of a pattern is given by a_{gh}=$(1/GH)\sum_{d=0}^{H-1}\sum_{e=0}^{G-1} x_{de} W_{gh}(d,e)$, where g=0,1,...,G-1 and h=0,1,...,H-1. The value x_{de} is the gray level of a pattern in the e-th row cell in the d-th column, $W_{gh}(d,e)$ is the value 1 or -1 of the g, h-th order of the two-dimensional discrete Walsh function in the e-th row cell in the d-th column, and a_{gh} is the two-dimensional Walsh spectrum. If there are just two gray levels: for instance "black" and "white," x_{de} is usually represented by 1 and 0 (Fig. 2a. See also p. 573 in Wolfram (2002)).

Symmetric component P_k (k=1, 2, 3, 4), quantifying the four types of symmetry, is given by $P_k = \sum_{gh} (a_{gh})^2 / K$, where $K = \sum_{h=0}^{H-1} \sum_{g=0}^{G-1} (a_{gh})^2 - (a_{00})^2$ and $\sum_{k=1}^{4} P_k = 1$ (Fig. 2b). Vertically symmetric component P_1 is given when g=even and h=odd. Horizontally symmetric component P_2 is given when g=odd and h=even. Centrosymmetric component P_3 is given when g=odd and h=odd. Double symmetric component P_4 is given when g=even and h=even. The sum is taken over all ordered pairs (g, h) for $0 \le g \le G$-1 and $0 \le h \le H$-1 where a_{00} is excepted. When the entropy function in information theory is applied to P_k (k=1, 2, 3, 4), symmetropy S is defined by

$$S = -\sum_{k=1}^{4} P_k \log_2 P_k. \tag{2}$$

S ranges from 0 to 2 bits. If the value of a certain component is larger than the values of the other three components, the pattern is rich in symmetry related to the certain component. In this case, Eq. (2) shows that S decreases. On the other hand, if the values of the four components are almost equal each other, the pattern is poor in symmetry and S increases. In the pattern consists of only white cells (i.e., blank cells), we define S as 2.0 bits.

We regard the AE events as circles with finite diameter. Following previous studies (e.g., Nanjo et al., 2000; 2005; 2006), the spatial patterns of AE were covered with $2^5 \times 2^6$ cells. If we find a part of or whole of one or more of circles in a cell of (i, j), then $x_{ij} = 1$, otherwise $x_{ij} = 0$. In this case, we can estimate the symmetropy of fracture patterns by using Eq. (2).

2.3 Methods II: Partial symmetropy

In general, the goodness and the complexity of a pattern seem to be directly related not only to the amount of whole symmetropy but also to the amount of PS in the pattern (Yodogawa, 1982). However, in the previous studies on fracture patterns, the whole symmetropy has been the only indicator of estimating the symmetry of fracture patterns (e.g., Nanjo et al., 2000; 2005; 2006). Then, we now define a measure of PS and another related measure of fracture patterns based on Yodogawa (1982).

Let A be any $M \times N$ pattern, where $2^{r+1} \ge M \ge 2^r$ and $2^{t+1} \ge N \ge 2^t$ and r and t is a positive integer. To obtain the measure of PS, some observation windows are introduced. The observation windows are the $2^k \times 2^l$ (k=1,2,...,r and l=1,2,...,t) rectangular regions through which the pattern A is observed at all possible distinct window positions. At each window position in the pattern A, we calculate the symmetropy of each subpattern observed through the $2^k \times 2^l$ window. The mean value of PS (averaged over all possible window positions), and its standard deviation are calculated for each window size. In this paper, they are denoted by $S^{k,l}$ and $\sigma^{k,l}$, respectively. The value of $S^{k,l}$ can be considered as a measure of PS, and the value of $\sigma^{k,l}$ are introduced with the intention of estimating the homogeneity of the pattern A for each window size. As we will see in Sections 3 and 4, the relationship between $S^{k,l}$ and $\sigma^{k,l}$ can be used to distinguish the regular pattern from the random pattern.

Take Fig. 3 for illustrative examples. Fig. 3a is a $2^3 \times 2^4$ random pattern. Fig. 3b is the result of the observation windows $2^1 \times 2^2$. The PS of each subpattern observed through the $2^1 \times 2^2$ window is represented by matrix ((8-2+1)×(16-4+1))=7×13. From the matrix, the mean value of the PS and its standard deviation are calculated: $S^{1,2}$=1.50 bits and $\sigma^{1,2}$=0.37 bits. In a similar fashion, we obtain $S^{2,3}$=1.86 bits and $\sigma^{2,3}$=0.10 bits (Fig. 3c); $S^{3,4}$=1.97 bits and $\sigma^{3,4}$=0 bits (Fig. 3d).

In this paper, we cover the fracture pattern with $2^5 \times 2^6$ cells, and calculate $S^{k,k+1}$ and $\sigma^{k,k+1}$ (k=1,...,5). Before considering the fracture pattern, we take up two extreme cases of patterns: random pattern and straight regular pattern (Figs. 4a and 5a). This leads us to clarify the geometrical meaning of the results of the fracture pattern. In the random pattern, we shift the ratio of black area to white area from 1:1 to 1:10. In the straight regular pattern, we shift the width of the pattern from 2 to 30. We calculate $S^{k,k+1}$ and $\sigma^{k,k+1}$ (k=1,...,5) in each pattern, and investigate the relationship between $S^{k,k+1}$ and $\sigma^{k,k+1}$.

3 Results

Fig. 6 shows that the mean value of the PS $S^{k,k+1}$ and its standard deviation $\sigma^{k,k+1}$ plotted against the scale k (=1,...,5). Fig. 7 shows the variation in $S^{k,k+1}$, $\sigma^{k,k+1}$ and the fractal dimension D of the AE patterns with the evolution of the fracturing process. Since $\sigma^{5,6}$=0 bits in the pattern covered with $2^5 \times 2^6$ cells, we excluded it from the plot. According to Lockner et al., (1992), fault nucleation occurs in the time step 4, i.e., pre-nucleation occurs before the step 4; propagation occurs after the step 4. The most distinguished feature of the result is as follows. Fig. 7a shows that the value of $S^{k,k+1}$ decreases abruptly at the nucleation phase (the step 4). Fig. 7b shows that the value of $\sigma^{k,k+1}$ increases abruptly at the nucleation phase (the step 4). On the other hand, Fig. 7c shows that the value of D increases gradually up to the last step as a whole, i.e., it does not show a sharp change at the nucleation phase (the step 4). Except for the step 8, the value of D falls in the range 1.0 to 1.6, which is equal to the accepted fractal range of fracture rocks: $1.0 \leq D \leq 1.6$ (e.g., Kagan and Knopoff, 1980; Hirata et al., 1987; Nakamura and Nagahama, 2001).

It is found from Fig. 7a that (I) during the pre-nucleation phase (the steps 2 $\sim$ 4), $S^{k,k+1}$ (k=1, ..., 5) show almost the same value regardless of the scale k; (II) during the propagation phase (the steps 5 $\sim$ 8), $S^{k,k+1}$ vary with the scale. Fig. 7b also shows that the variations of $\sigma^{k,k+1}$ among the scales k during the pre-nucleation phase are smaller than those during the propagation phase. It is found from Figs. 6 or 7b that the relationship between variations of $\sigma^{k,k+1}$ and the scale k is given by the following scaling law:

$$\sigma^{k,k+1} = a \left(2^k\right)^{-b}, \tag{3}$$

where a and b are constants vary with the time step. In the right side of this equation, we use the window size 2^k but not the index k, because the former corresponds to the concept of the size in the fractal analysis such as r in Eq.(1). The values of b are shown in Fig. 7c. Eq.(3) is one of the fractal distributions, so the index b can be recognized as the fractal dimension for $\sigma^{k,k+1}$. As shown in Fig. 7c, there is no correlation between b and D.

Next, we derive the relationship between $S^{k,k+1}$ and $\sigma^{k,k+1}$ in the following two cases: (I) the scale k is fixed; (II) k is shifted.

When the scale is fixed, by using the data on Figs. 7a and 7b, we can obtain

$$\sigma^{4,5} = -0.74 S^{4,5} + 1.48 \left(R^2 = 0.95\right), \tag{4}$$

$$\sigma^{3,4} = -1.77 S^{3,4} + 3.54 \left(R^2 = 0.87\right), \tag{5}$$

$$\sigma^{2,3} = -1.84 S^{2,3} + 3.73 \left(R^2 = 0.98\right), \tag{6}$$

$$\sigma^{1,2} = -1.19 S^{1,2} + 2.53 \left(R^2 = 0.92\right), \tag{7}$$

where R^2 is the regression coefficient. As can be seen from the above equations, $\sigma^{k,k+1}$ is negatively proportional to $S^{k,k+1}$ when the scale is fixed.

Next let us consider the case when the scale k is shifted. Before considering the natural pattern, we take up two artificial patterns: random pattern and straight regular pattern (Figs. 4a and 5a). Fig. 4a is a random pattern, where the ratio of black area to white area is 1:1. Fig. 5a is a straight regular pattern, where the width of the pattern is 2. Figs. 4b and 5b show the values of $S^{k,k+1}$ and $\sigma^{k,k+1}$ (k=1,...,5) for each pattern. In the random pattern, the value of $S^{k,k+1}$ shows a negative $\sigma^{k,k+1}$ dependence (Fig. 4b). On the other hand, in the regular pattern, the value of $S^{k,k+1}$ shows a positive $\sigma^{k,k+1}$ dependence as a whole (Fig. 5b). In a similar fashion, we calculate the value of $S^{k,k+1}$ and $\sigma^{k,k+1}$ for other cases, and find that (I) the negative dependence in the random pattern holds regardless of the black-white ratio, and the positive dependence in the regular pattern also holds regardless of the width of the straight pattern; (II) the dependence are expressed by the linear relation whose value of slope and intercept are summarized in Figs. 8a and 8b. Here, the black-white ratio is normalized as dividing white ratio by black ratio. In the analysis of the regular patterns, we exclude the data on k=4 from the least-squares fitting, because it is far from the regression line. Fig. 8a shows that in the random pattern the value of the intercept remains fairly constant 2.0, and the absolute value of the slope $|a_r|$ follows

$$|a_r| = 1.5\exp(-0.13r) \text{ (for } r \geq 1) \ \left(R^2 = 0.99\right), \tag{8}$$

$$|a_r| = 1.3r^{0.22} \text{ (for } r \leq 1) \ \left(R^2 = 0.95\right), \tag{9}$$

where r is (white ratio)$\div$(black ratio). We use the power law relation for $r \leq 1$, because the R^2-value is higher than that of the exponential relation. Similar to the random pattern, Fig.8b shows that in the regular pattern the value of the intercept remains fairly constant zero, and the value of the slope a_s follows

$$a_s = 3.1\exp(-0.08w) \ \left(R^2 = 0.99\right), \tag{10}$$

where w is the width of the pattern.

To make it easily accessible the dependence in each scale, the negative dependence (the random pattern) is blacked out, and the positive dependence (the regular pattern) is whited out as shown in Figs. 4c and 5c. As we will see, this "barcode" expression is a useful tool for quantification of the evolution of fracturing process, in which the dependence is not so simple in comparison with the two extreme cases of patterns: random and regular. Based on Fig. 6, we give the "barcode" expression for the fracturing process illustrated in Fig. 9. The first stage (1, 2) and the last stage (7, 8) indicate the existence of a lower degree of organization, and the midst stage ($3 \sim 6$) indicates a higher degree of organization.

In summary of this section, we have found that: (i) The value of $S^{k,k+1}$ and $\sigma^{k,k+1}$ shows a sharp change at the nucleation phase. On the other hand, the value of D increases gradually up to the last step as a whole; (ii) The variations of $S^{k,k+1}$ and $\sigma^{k,k+1}$ among the scales k during the pre-nucleation phase are smaller than those during the propagation phase; (iii) When the scale k is fixed, $\sigma^{k,k+1}$ is negatively proportional to $S^{k,k+1}$; (iv) When the scale k is shifted, $S^{k,k+1}$ shows a negative $\sigma^{k,k+1}$ dependence in the random pattern, and a positive $\sigma^{k,k+1}$ dependence as a whole in the regular pattern; (v) We introduce the "barcode" expression for the fracturing process to show a higher and a lower degree of organization during the process.

4 Discussion

It is important for the basic research on predicting earthquakes to find out the quantity that can be used to watch the timing of nucleation's occurrence in fracturing process (e.g., Ito and Matsuzaki, 1990; Lockner et al., 1992). Here, we discuss this point based on the results obtained in this paper. Nanjo et al., (2000) calculated the symmetropy of AE patterns on the scale k=5 based on Hirata et al., (1987)'s data, and found that the symmetropy decreases with the evolution of the fracturing process. In this paper, we calculated the PS on the various scale k=1,...,5 based on Lockner et al., (1992)'s data as shown in Fig. 7a. Taking notice of the fist step 1 and the last step 8, the mean value of the PS $S^{k,k+1}$ decreases regardless of the scale, which is consistent with Nanjo et al., (2000)'s result. In the process of being fractured, however, the change in $S^{k,k+1}$ is not so simple: $S^{k,k+1}$ remains almost constant during the pre-nucleation phase and shows a sharp fall at the nucleation phase (the step 4). Fig. 7b shows that the standard deviation $\sigma^{k,k+1}$ undergoes the same type of process as the PS, but the pattern is reversed as indicated by Eqs. (4)$\sim$(7). On the other hand, the fractal dimensions D and b do not show a sharp change at the nucleation phase (the step 4).

These results imply that the mean value of the PS or its standard deviation are better at finding the occurrence of the nucleation than the fractal dimensions are.

Next, let us consider the physical meaning of the variations of $S^{k,k+1}$ during the fracturing process. According to the SOC fault simulation performed by Nanjo et al., (2005; 2006), the symmetropy on the scale k=5 takes almost maximum value during subcritical state: 1.9$\sim$2.0 bits, and takes various decreasing values during critical state: 1.52$\sim$1.94 bits. On the other hand, as shown in Fig. 7a, the symmetropy on the scale k=5 takes almost maximum value during the pre-nucleation phase, and various decreasing values during the propagation phase. Therefore, it is found that the pre-nucleation phase corresponds to the subcritical states, and the propagation phase to the critical state. This one-to-one correspondence holds regardless of the scale except for k=1.

In this paper, the PS is characterized by calculating the mean value of the PS $S^{k,k+1}$ for the scale k. When k is shifted, the value of $S^{k,k+1}$ increases in the random pattern (Fig. 4b), and decreases in the straight regular pattern (Fig. 5b). Let us consider the meaning of large and small values of $S^{k,k+1}$ in terms of scaling. (i) On the small scale of the random pattern (especially, $k = 1$), the regular pattern is created by happenstance, i.e., a certain symmetry component predominates among the other components. In this case, the value of $S^{k,k+1}$ decreases as indicated by Eq. (2). (ii) On the large scale of the random pattern, there is no regularity. That is, the values of the symmetry component are almost equal each other, and the value of the $S^{k,k+1}$ increases. From (i) and (ii), the value of the $S^{k,k+1}$ in the random pattern increases with an increase in the scale k (e.g., Fig. 4b). (iii) On the small scale, the large scale regular pattern cannot be recognized. Therefore, the value of $S^{k,k+1}$ is large. (iv) On the large scale, the regular pattern can be recognized, and the value of $S^{k,k+1}$ is small. From (iii) and (iv), the value of the $S^{k,k+1}$ in the regular pattern decreases with an increase in the scale k (e.g., Fig. 5b). These findings lead us to a suggestion that the mean value of the PS is useful to analyze the random and the regular pattern. It is hard for the fractal geometry to perform the same analysis.

Now, we have found that the mean value of the PS $S^{k,k+1}$ is not irrelevant to its standard derivative $\sigma^{k,k+1}$. Especially, in the random pattern, the change in $S^{k,k+1}$ is negatively proportional to the change in $\sigma^{k,k+1}$ (Figs. 4b and 4c), and in the straight regular pattern, the former is proportional to the later as a whole (Figs. 5b and 5c). Theses negative or positive dependencies are expressed by the linear relation whose value of slope and intercept obey Eqs. (8), (9) and (10). Eqs. (8) and (10) show that the value of the slope increases with the percentage of black area increases. Since we consider the fracture patterns, we take up only straight pattern as the regular pattern. If the positive dependence, however, holds in other regular pattern, we may say that the relationship between $S^{k,k+1}$ and $\sigma^{k,k+1}$ is a simple indicator of distinguishing between the regular and the random patterns. In any case, the negative or the positive dependencies are the useful tool to investigate a complex pattern consists of regular and random patterns such as fracturing process, which we will do this below.

We have investigated the scale dependence of the relationship between $S^{k,k+1}$ and $\sigma^{k,k+1}$ for fracture patterns, and suggested a "barcode" expression of this dependence illustrated in Fig. 9. This "barcode" expression simplifies the complicated fracturing process down to three easy steps: (i) a lower degree of organization (1,2); (ii) a higher degree of organization (3 $\sim$ 6); (iii) a lower degree of organization (7, 8). A higher degree of organization in the step (ii) may be due to the occurrence of the nucleation (4). Steps (i) and (iii) imply that the final phase of the propagation is random pattern as well as the early phase of the pre-nucleation. From the geometric patterns of fracturing such as Fig. 1, we often intuit that the fracturing is a transition from the non-order to the order. Fig. 9, however, shows that the order (3 $\sim$ 6) is sandwiched in between the non-orders (1, 2) and (7, 8). This is a new interpretation of the fracturing process in the sense of the PS. It is an interesting that this sandwich structure cannot be discovered by the fractal dimensions and the separate observation of $S^{k,k+1}$ and $\sigma^{k,k+1}$ (Fig. 6).

Finally, we apply the Tsallis statistics (Tsallis, 1988) to the PS of fracturing process. As a result, the latter concept can be used for nonextensive situations that thought to be associated with earthquake fracturing (Kalimeri et al., 2008). Eq. (2) shows that S satisfies extensivity if correlations within the system considered are essentially local or the subsystems are statistically (quasi-)independent. In such cases, the system is called extensive (Kalimeri et al., 2008). An example includes Boltzman-Gibbs (BG) entropy. Following Kalimeri et al., (2008), we assume that the system under study, due to the appearance of strong correlations and information transition across the focal area just before a large earthquake or across the experimental rock just before the ultimate fracture, possibly violates the BG statistics. Thus extensive situation may be far negligible at all scales. In such cases, the entropy may be nonextensive. Inspired by multifractal concepts, Tsallis (1988) has proposed a generalization of the BG statistical mechanics. We apply this generalization to symmetropy and call the generalized one as Tsallis symmetropy S_q^k :

$$S_q^k = \frac{1 - \sum_{i=1}^{4} P_i^q}{q-1} \log_2 e \times 2 \left(\frac{1 - 4(0.25)^q}{q-1} \log_2 e \right)^{-1}, \tag{11}$$

where q is an index which leads to a noextensive statistics (a measure of the nonextensivity of the system). Using $(\cdots)^q$=$(\cdots)(\cdots)^{q-1}$=$(\cdots)$exp[(q-1)ln$(\cdots)$]$\simeq$$(\cdots)$(1+(q-1)ln$(\cdots)$) at $q\to1$, we reduce the usual symmetropy in Eq. (1):$S_1^k \to S^k$. Since S^k is extensive and S_q^k is nonextensive, we define the following quantity to measure the degree of nonextensivity:

$$\Delta S_q^k = \frac{S_q^k - S^k}{S^k}. \tag{12}$$

ΔS_q^k increases with an increase in the Tsallis symmetropy. In the case of q=5 and k=1,...,5, we calculate ΔS_q^k of fracturing process illustrated in Figs. 10a and 10b. For the large scale symmetropy (k=3, 4, 5), Fig. 10a shows that the value of ΔS_q^k increases abruptly after the nucleation phase (the step 4). This means that the subsystem of the system considered becomes statistically dependent immediately after the nucleation phase. On the other hand, for the small scale symmetropy (k=1, 2), Fig. 10b shows that the value of ΔS_q^k simply increases with the fracturing process. This implies that the size of the interactive subsystem related to the nucleation may have a lower limit.

The analysis in the present paper leads us to the following conclusions: (i) $S^{k,k+1}$ shows a sharp fall at the nucleation phase. Therefore, by noting the PS, we can distinguish the nucleation phases from the other phases such as the pre-nucleation and the propagation phases; (ii) $S^{k,k+1}$ ($k = 2{\sim}5$) takes almost maximum value (2.0 bits) during the pre-nucleation, and various decreasing values (1.68$\sim$1.95 bits) during the propagation phase. This implies that the fracturing process is a type of phase transitions from the subcritical state to the critical states; (iii) When the scale k is shifted to larger one, $S^{k,k+1}$ increases in the random pattern and decreases in the straight regular pappern. On the other hand, $\sigma^{k,k+1}$ decreases in the both patterns. Therefore, the relationship between $S^{k,k+1}$ and $\sigma^{k,k+1}$ is a simple indicator of distinguishing between the random pattern and the straight regular pattern; (iv) In the evolution of the fracturing pattern, the sandwich structure consists of order and non-order can be observed. This structure has not been recognized in the previous studies; (v) We apply the Tsallis nonextensive statistics to the concept of the symmetropy and define the Tsallis symmetropy. The degree of nonextensivity on a large scale ($k = 3, 4, 5$) shows that the subsystem becomes statistically dependent immediately after the nucleation.

Acknowledgements

We wish to thank R. Teisseyre and R. Okajima for their helpful comments.

References

Contoyiannis, Y.F., and Eftaxias, K., 2008. Tsallis and Levy statistics in the preparation of an earthquake. Nonlinear Process Geophys., 15: 379-388.

Enya, O., 1901. Note on after-shocks of earthquakes. Rep. Earthquake Invest. Comm., 35: 35-56 (in Japanese).

Hirata, T., Satoh, T., and Ito K., 1987. Fractal structure of spatial distribution of microfracturing in rock. Geophys. J. R. Astron. Soc., 90: 369-374.

Ito, K., and Matsuzaki, M., 1990. Earthquakes as self-organization critical phenomena. J. Geophys. Res., 95: 6853-6860.

Kagan, Y.Y., and Knopoff, L., 1980. The spatial distribution of earthquakes: The two-point correlation function. Geophys. J. R. Astron. Soc., 62: 303-320.

Kalimeri, M., Papadimitriou, C., Balasis, G., and Eftaxias, K., 2008. Dynamical complexity detection in pre-seismic emissions using nonadditive Tsallis entropy. Physica A, 387: 1161-1172.

Locker, D.A., Byerlee, J.D., Kuksenko, V., Ponomarev, A. and Sidorin, A., 1992, Observations of quasistatic fault growth from acoustic emissions. In: B. Evans and T.-F. Won (Editors). Fault Mechanics and Transport Properties of Rocks, 1-31.

Mandelbrot, B.B., 1982. The Fractal Geometry of Nature. W.H. Freeman, New York, 460 pp.

Nakamura, N., and Nagahama, H., 2001. Changes in magnetic and fractal properties of fractured granites near the Nojima Fault, Japan. The Island Arc, 10: 486-494.

Nanjo, K., Nagahama, H., and Yodogawa, E., 2000. Symmetry properties of spatial distribution of microfracturing in rock. Forma, 15: 95-101.

Nanjo, K., Nagahama, H., 2004. Fractal properties of spatial distributions of aftershocks and active faults. Chaos Solitons Fractals, 19: 387-397.

Nanjo, K.Z., Nagahama, H., and Yodogawa, E., 2005. Symmetropy of fault patterns: quantitative measurement of anisotropy and entropic heterogeneity. Math. Geol., 37: 277-293.

Nanjo, K.Z., Nagahama, H., and Yodogawa, E., 2006. Symmetropy of earthquake patterns: asymmetry and rotation in a disordered seismic source. Acta Geophys. 54: 3-14.

Nishiyama, Y., Nanjo, K.Z., and Yamasaki, K., 2008. Geometrical minimum units of fracture patterns in two-dimensional space: Lattice and discrete Walsh functions. Physica A 387: 6252-6262.

Papadimitriou, C., Kalimeri, M., and Eftaxias, K., 2008, Nonextensivity and universality in the earthquake preparation process. Phys. Rev. E, 77: 036101/1-14.

Tsallis, C., 1988. Possible generalization of Boltzmann-Gibbs Statics. J. Stat. Phys., 52: 479-487.

Tsallis, C., 2002. Entropic nonextensivity: a possible measure of complexity. Chaos Solitons Fractals., 13: 371-391.

Turcotte, D.L., 1997. Fractals and Chaos in Geology and Geophysics 2nd ed. Cambridge University Press, New York, 398 pp.

Wolfram, S., 2002. A New Kind of Science. Wolfram Media, Campaign, IL, 1197 pp.

Yodogawa, E., 1982. Symmetropy, an entropy-like measure of visual symmetry. Percept. Psychophys, 32: 230-240.

Figure captions

Fig. 1. Examples of the spatial distribution of AE events occurring in a rock specimen (modified from Fig. 8 in Lockner et al., 1992). Plot of each set is view looking along-strike of eventual fracture plane. According to Lockner et al., (1992), fault nucleation occurs in step 4. For reference, the projection of the surface trace of the final fault plane is shown in step 1.

Fig. 2. (a) Examples of the two-dimensional discrete Walsh function for $M = N = 8$. Black represents +1 and white represents -1. (b) Four types of symmetry in the sense of the discrete Walsh function.

Fig. 3. A sample of PS. (a) A sample pattern covered by 8×16 cells. (b) The PS of the sample pattern in 2×4 observed window. $S^{1,2}$ and $\sigma^{1,2}$ are the mean value of the PS and its standard deviation, respectively. (c) The PS in 4×8 observed window. (d) The PS in 8×16 observed window.

Fig. 4. (a) A random pattern with the ration of black area to white area is 1:1. (b) The mean value of the PS $S^{k,k+1}$ and the standard deviation $\sigma^{k,k+1}$ plotted against the scale k. It is found that $S^{k,k+1}$ shows a negative $\sigma^{k,k+1}$ dependence. (c) A "barcode" expression of (b). The negative dependence is blacked out.

Fig. 5. (a) A straight regular pattern where the width of the pattern is 2. (b) $S^{k,k+1}$ and $\sigma^{k,k+1}$ plotted against the scale k. It is found that $S^{k,k+1}$ shows a positive $\sigma^{k,k+1}$ dependence as a whole. (c) A "barcode" expression of (b). The negative dependence is black out, and the positive dependence is white out.

Fig. 6. For the data on the AE patterns in rocks, we calculated the mean value of the PS $S^{k,k+1}$ and the standard deviation $\sigma^{k,k+1}$. $S^{k,k+1}$ and $\sigma^{k,k+1}$

are plotted against the scale k at each time step. In the first stage (the steps 1 and 2) and the last stage (the steps 7 and 8), there is a negative dependence. In the midst stage (the steps $3 \sim 6$), there is a positive dependence.

Fig. 7. The mean value of the PS $S^{k,k+1}$, the standard deviation $\sigma^{k,k+1}$ and the fractal dimensions D and b plotted against the step. The values of $S^{k,k+1}$ and $\sigma^{k,k+1}$ change abruptly at the nucleation phase (the step 4). On the other hand, the fractal dimensions do not show a sharp change at the nucleation.

Fig. 8. The negative and the positive dependence between $S^{k,k+1}$ and $\sigma^{k,k+1}$ are expressed by the linear relation. The values of slope and intercept for the linear relation plotted against (white ratio/black ratio) ($=r$) in the random pattern, and the width of the straight regular pattern ($=w$). The regression lines are expressed by Eqs. (8), (9) and (10).

Fig. 9. A "barcode" expression of Fig. 6. In the first stage (the steps 1 and 2) and the last stage (the steps 7, 8), there is a lower degree of organization (non-order). In the midst stage (the steps $3 \sim 6$), there is a higher degree of organization (order).

Fig. 10. The degree of nonextensivity defined by Eq. (12) plotted against the step. (a) In the large scale symmetropy (k=3, 4, 5), the degree of nonextensivity shows a sharp change at the nucleation (the step 4). (b) In the small scale symmetropy (k=1, 2), we cannot observe the sharp change at the nucleation.

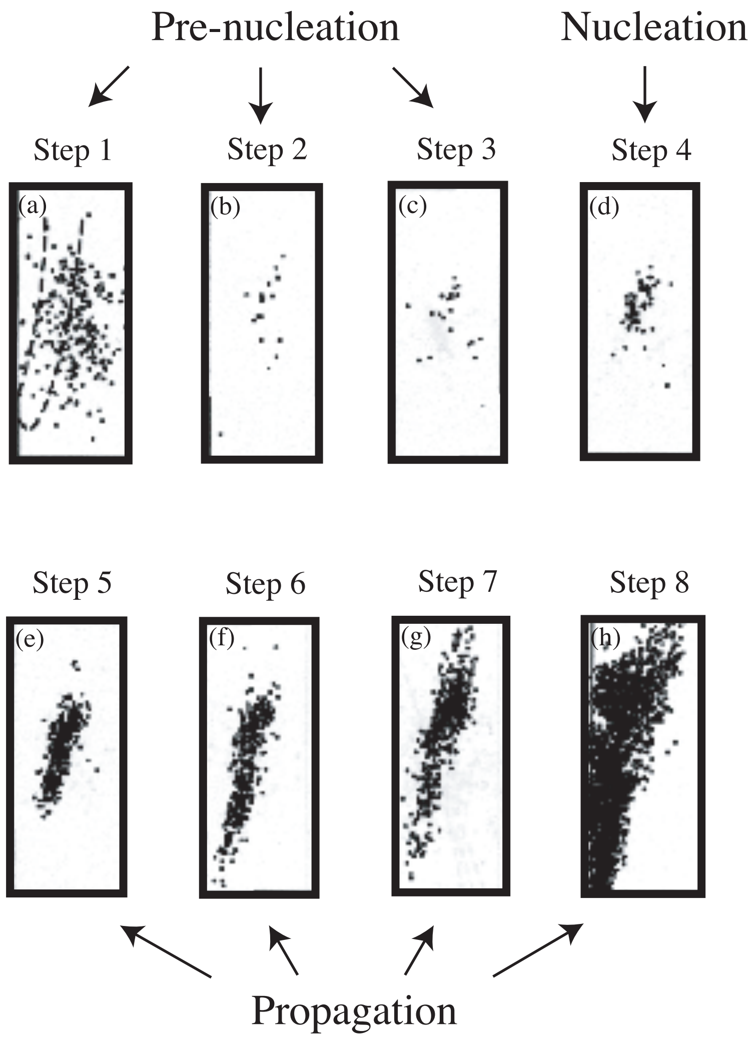
Pre-nucleation
Nucleation
Step 1
Step 2
Step 3
Step 4
(a)
(b)
(c)
(d)
Step 5
Step 6
Step 7
Step 8
(e)
(f)
(g)
(h)
Propagation

Fig.1

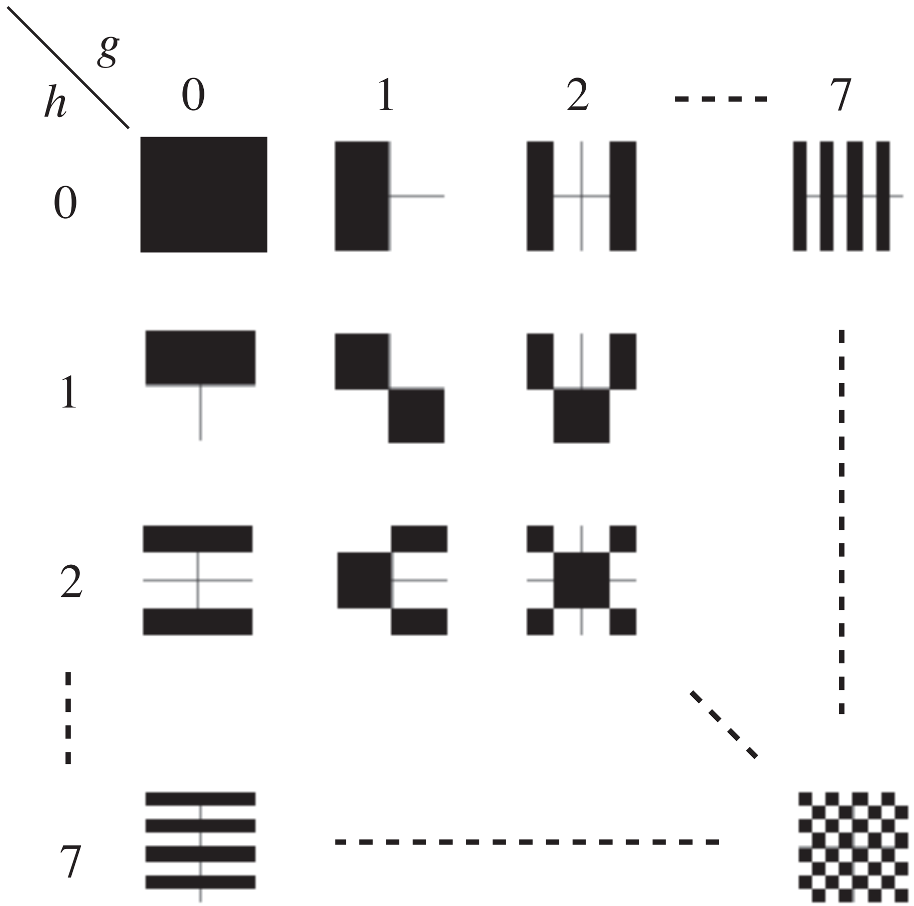
g
h
0
1
2
7
0
1
2
7

(a)

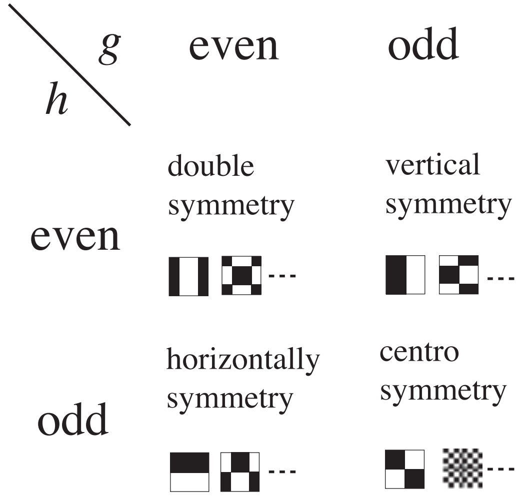
g
h
even
odd
even
double symmetry
vertical symmetry
odd
horizontally symmetry
centro symmetry

(b)

Fig.2

Figure3

Click here to download Figure(s): Fig3.pdf

(a) 8×16 random pattern

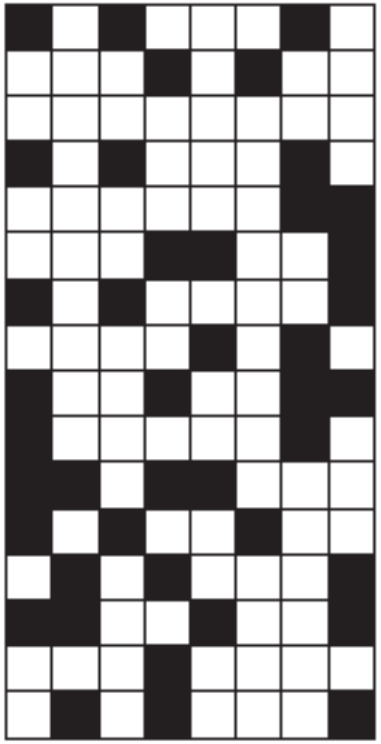

(b) window size = 2×4 (k=1 and l=2)

$$\begin{pmatrix} 0.92 & 0.92 & 1.43 & 1.95 & 1.95 & 1.43 & 0.92 \\ 1.95 & 1.95 & 1.59 & 1.95 & 1.95 & 1.43 & 1.43 \\ 1.95 & 1.95 & 1.59 & 0.92 & 1.95 & 0.92 & 2.00 \\ 0.92 & 0.92 & 1.43 & 0.92 & 1.95 & 1.59 & 1.43 \\ 1.95 & 1.95 & 0.92 & 1.43 & 1.59 & 0.92 & 1.43 \\ 1.59 & 1.95 & 1.43 & 2.00 & 1.59 & 1.59 & 1.43 \\ 1.43 & 1.95 & 1.59 & 0.92 & 1.95 & 1.43 & 1.43 \\ 1.00 & 1.95 & 1.59 & 2.00 & 0.92 & 1.43 & 2.00 \\ 1.43 & 1.59 & 1.43 & 1.43 & 1.59 & 1.43 & 1.43 \\ 1.43 & 1.43 & 1.43 & 1.43 & 0.92 & 1.59 & 0.92 \\ 0.92 & 1.00 & 1.43 & 2.00 & 1.43 & 1.95 & 1.59 \\ 2.00 & 1.43 & 1.43 & 1.43 & 1.59 & 1.95 & 0.92 \\ 1.00 & 1.43 & 1.43 & 1.00 & 1.95 & 2.00 & 1.43 \end{pmatrix} \longrightarrow \begin{matrix} S^{1,2} = 1.50 \\ \sigma^{1,2} = 0.37 \end{matrix}$$

(c) window size = 4×8 (k=2 and l=3)

$$\begin{pmatrix} 1.83 & 1.89 & 1.92 & 1.77 & 1.82 \\ 1.65 & 1.77 & 1.83 & 1.95 & 1.91 \\ 1.92 & 1.68 & 1.91 & 1.95 & 1.88 \\ 1.93 & 1.99 & 1.92 & 1.95 & 1.91 \\ 1.95 & 1.96 & 1.56 & 1.86 & 1.89 \\ 1.77 & 1.88 & 1.68 & 1.88 & 1.86 \\ 1.95 & 1.79 & 1.85 & 1.82 & 1.86 \\ 1.88 & 1.74 & 1.75 & 1.72 & 1.93 \\ 1.79 & 1.93 & 1.91 & 1.95 & 1.95 \end{pmatrix} \longrightarrow \begin{matrix} S^{2,3} = 1.86 \\ \sigma^{2,3} = 0.10 \end{matrix}$$

(d) window size = 8×16 (k=3 and l=4)

$$\begin{pmatrix} 1.97 \end{pmatrix} \longrightarrow \begin{matrix} S^{3,4} = 1.97 \\ \sigma^{3,4} = 0 \end{matrix}$$

Fig.3

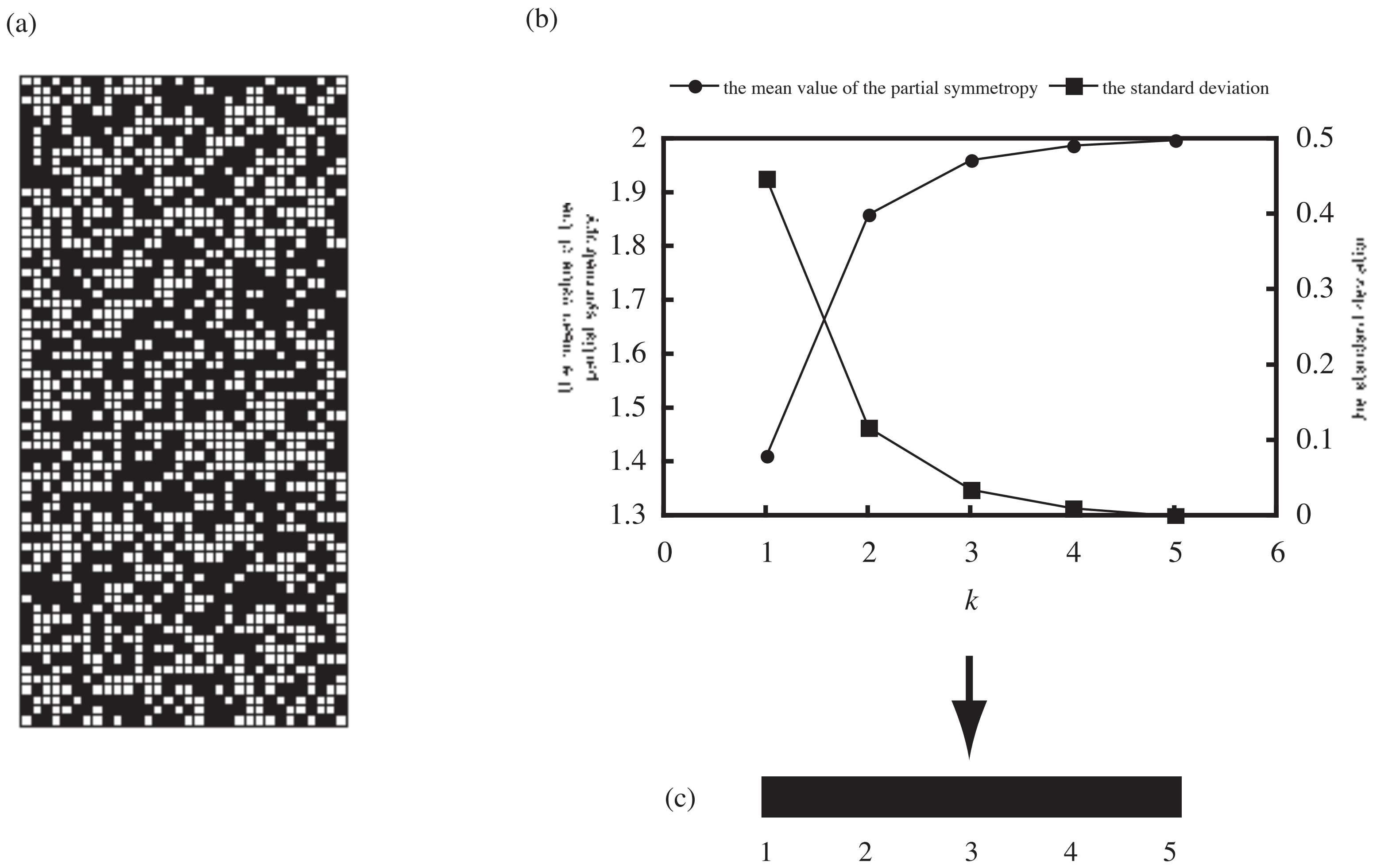
(a)
(b)
the mean value of the partial symmetropy
the standard deviation
2
1.9
1.8
1.7
1.6
1.5
1.4
1.3
0.5
0.4
0.3
0.2
0.1
0
0 1 2 3 4 5 6
k
(c)
1 2 3 4 5

Fig.4

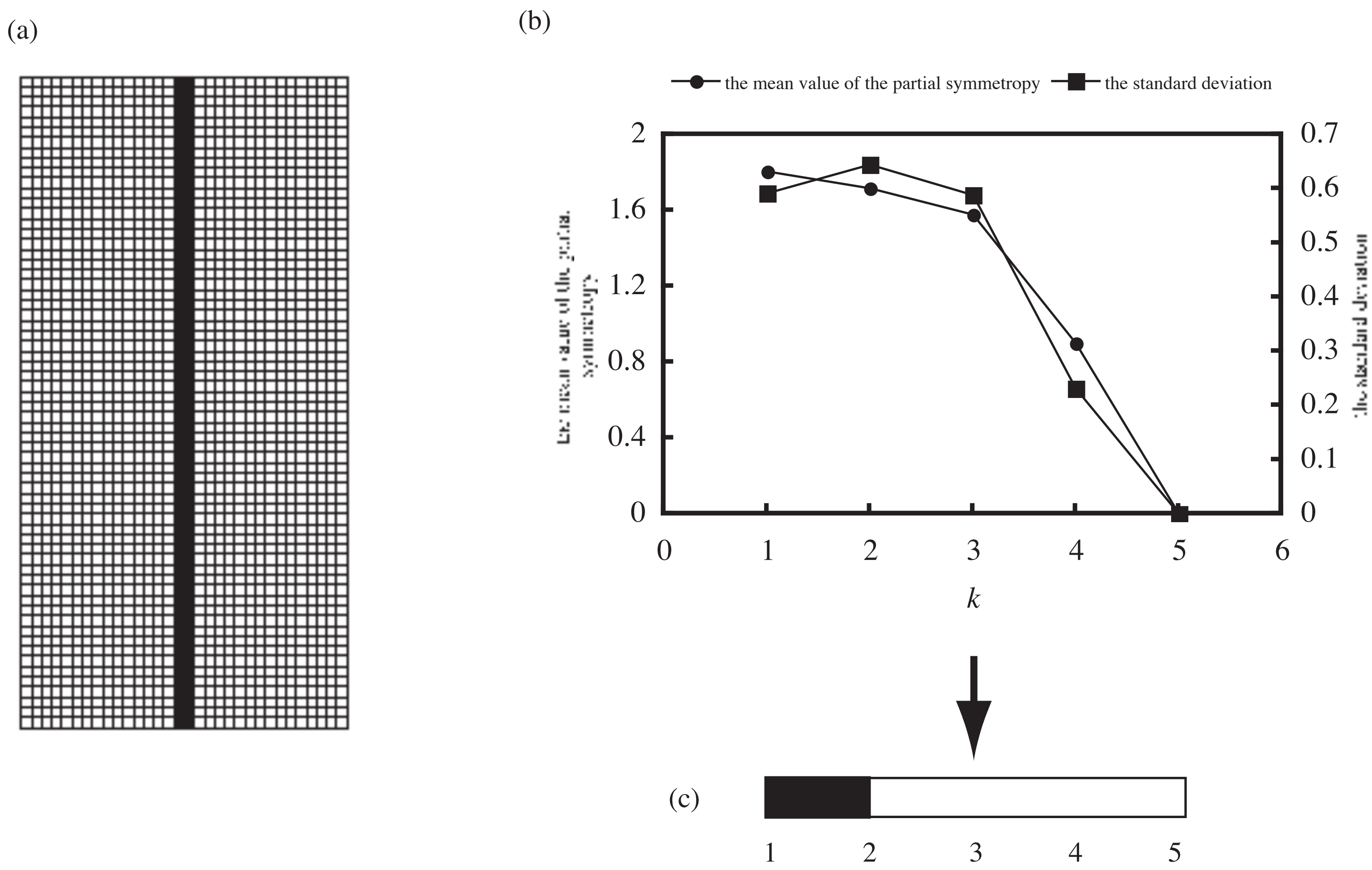
(a)
(b)
the mean value of the partial symmetropy
the standard deviation
2
1.6
1.2
0.8
0.4
0
0.7
0.6
0.5
0.4
0.3
0.2
0.1
0
0 1 2 3 4 5 6
k
(c)
1 2 3 4 5

Fig.5

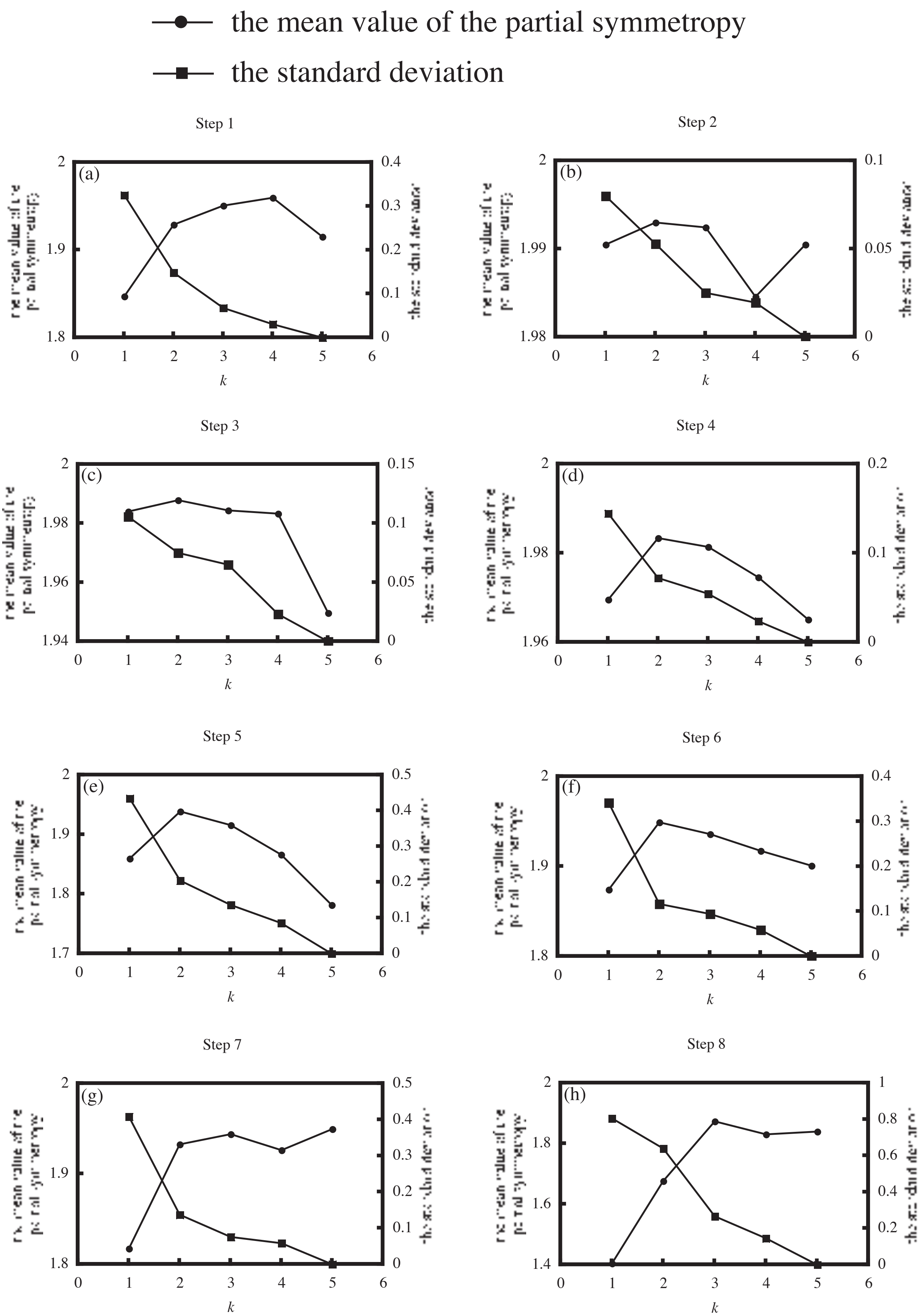
the mean value of the partial symmetropy
the standard deviation
Step 1
(a)
k
Step 2
(b)
k
Step 3
(c)
k
Step 4
(d)
k
Step 5
(e)
k
Step 6
(f)
k
Step 7
(g)
k
Step 8
(h)
k

Fig.6

Figure7
Click here to download Figure(s): Fig7.pdf

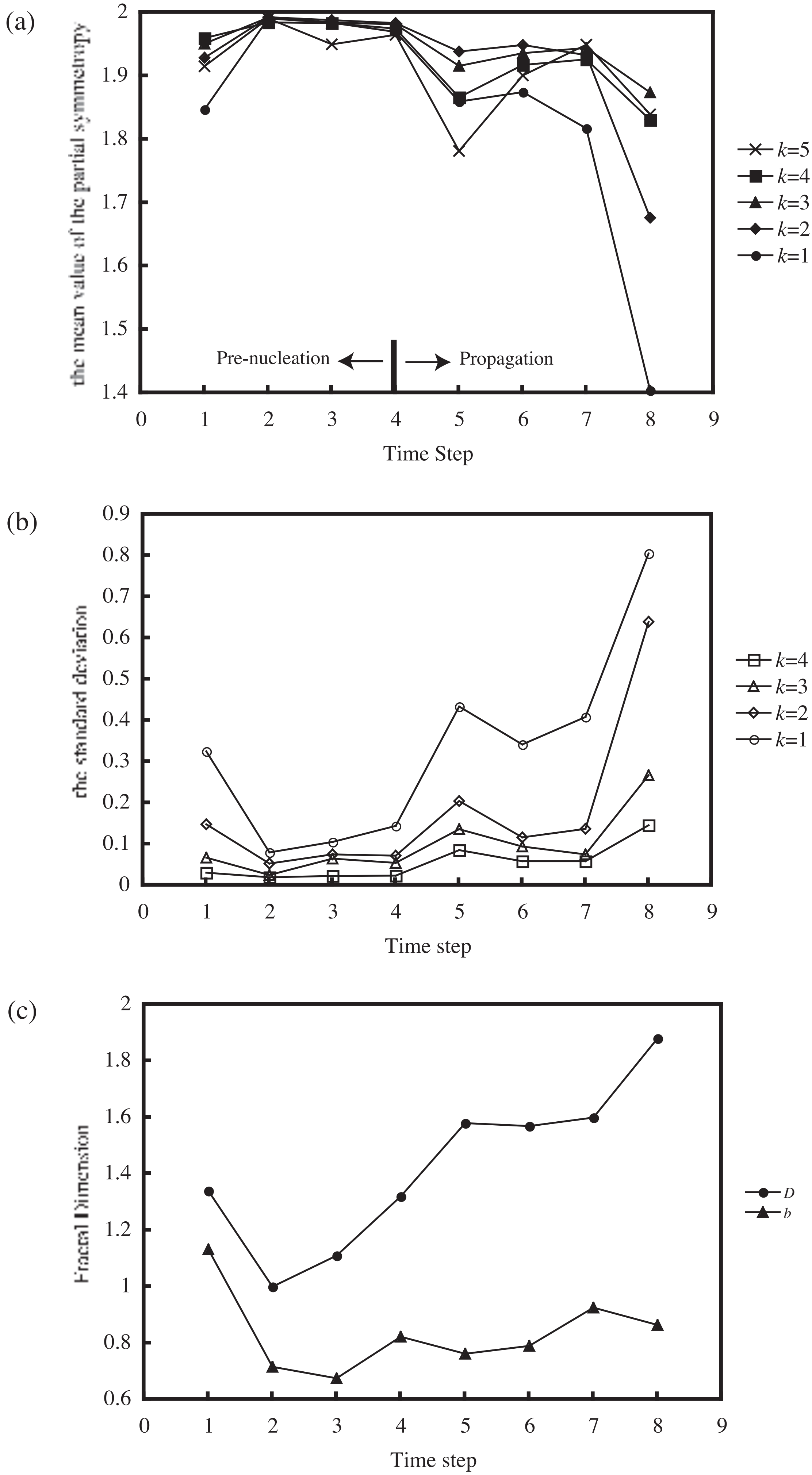

Fig.7

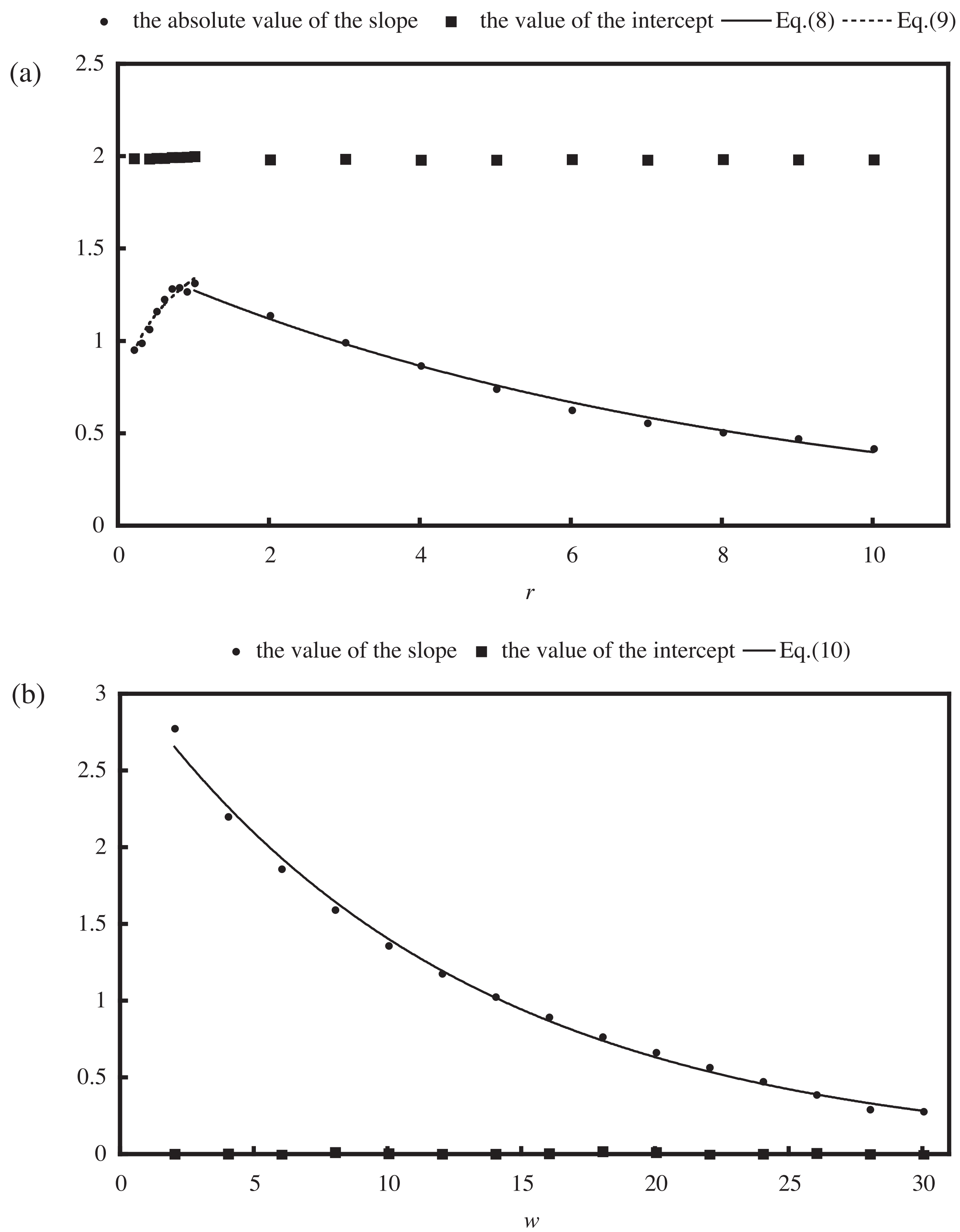
the absolute value of the slope
the value of the intercept
Eq.(8)
Eq.(9)
(a)
2.5
2
1.5
1
0.5
0
0
2
4
6
8
10
r
the value of the slope
the value of the intercept
Eq.(10)
(b)
3
2.5
2
1.5
1
0.5
0
0
5
10
15
20
25
30
w

Fig.8

Figure9
Click here to download Figure(s): Fig9.pdf

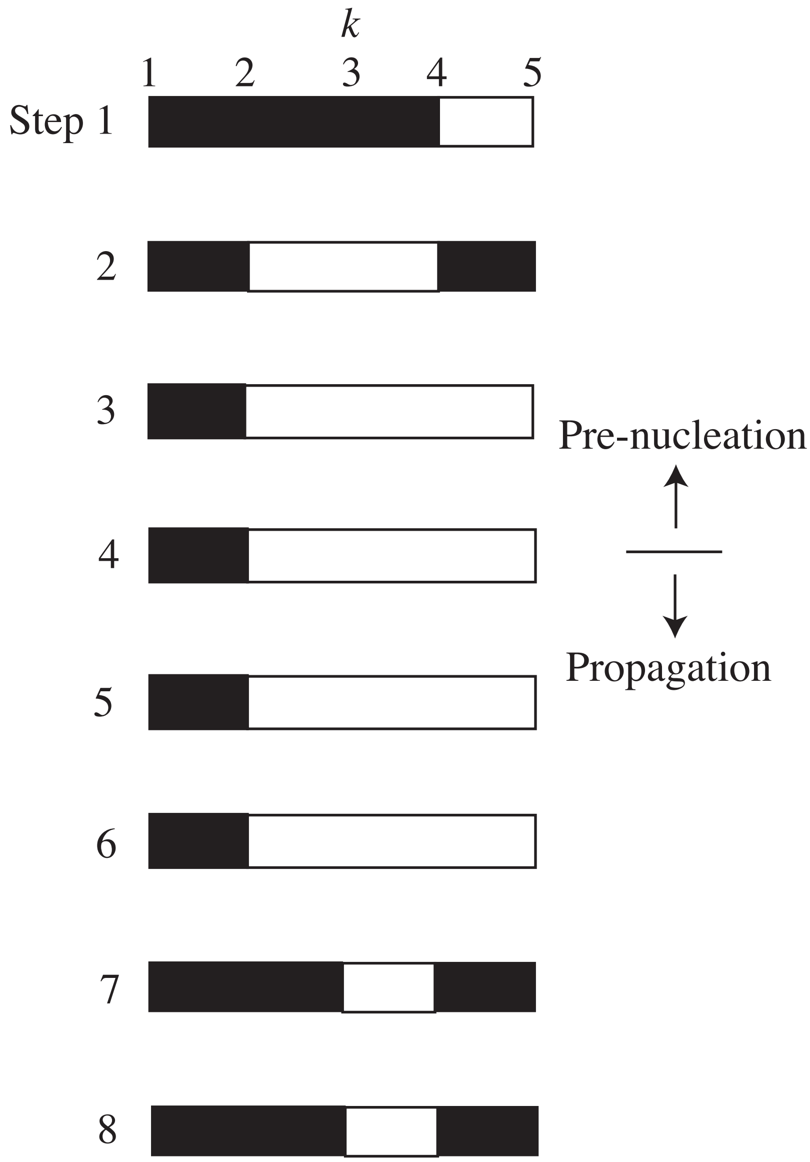

Fig.9

Figure10
Click here to download Figure(s): Fig10.pdf

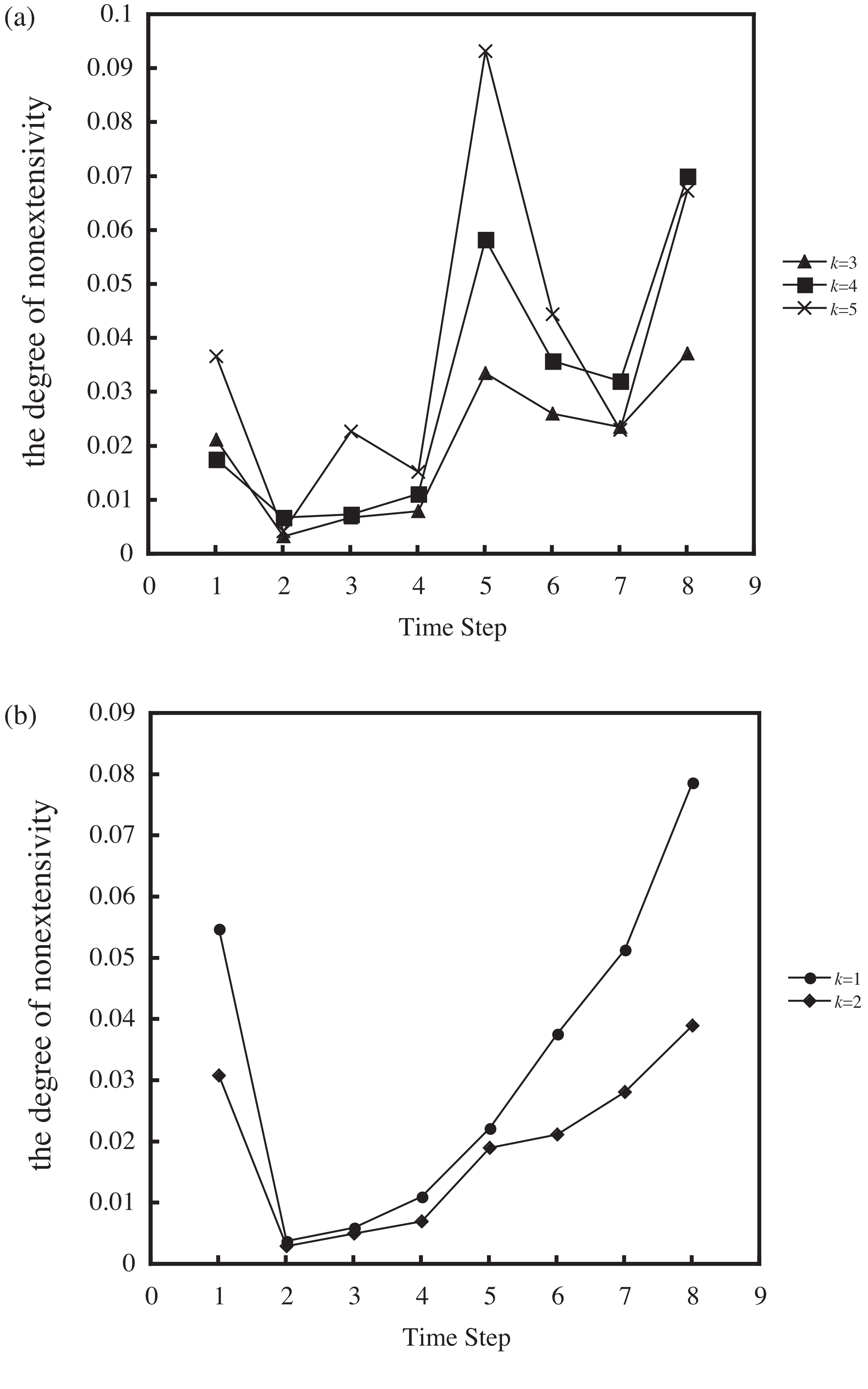

Fig.10